Nanostructured math xmlns="http://www.w3.org/1998/Math/MathML" display="inline" overflow="scroll">mrow>mi>Ga /mi>mi>As/mi>/mrow>/math>/(math xmlns="http://www.w3.org/1998/Math/MathML" display="inline" overflow="scroll">mi>Al/mi>mo>, /mo>mi>Ga/mi>/math>)math xmlns="http://www.w3.org/1998/Math/MathML" display="inline" overflow="scroll">mi>As/mi>/math> Waveguide for Low-Density Polariton Condensation from a Bound State in the Continuum

F. Riminucci, V. Ardizzone, L. Francaviglia, M. Lorenzon, C. Stavrakas, S. Dhuey, A. Schwartzberg, S. Zanotti, D. Gerace, K. Baldwin, L. N. Pfeiffer, G. Gigli, D. F. Ogletree, A. Weber-Bargioni, S. Cabrini, and D. Sanvitto

Phys. Rev. Applied **18**, 024039 — Published 15 August 2022

DOI: 10.1103/PhysRevApplied.18.024039

Nanostructured GaAs/(Al,Ga)As waveguide for low-density polariton condensation from a bound state in the continuum

F. Riminucci,[1,2] V. Ardizzone,[3] L. Francaviglia,[1] M. Lorenzon,[1] C. Stavrakas,[1] S. Dhuey,[1] A. Schwartzberg,[1] S. Zanotti,[4] D. Gerace,[4] K. Baldwin,[5] L. N. Pfeiffer,[5] G. Gigli,[2,3] D. F. Ogletree,[1] A. Weber-Bargioni,[1] S. Cabrini,[1] and D. Sanvitto[3,*]

[1] *Molecular Foundry, Lawrence Berkeley National Laboratory, One Cyclotron Road, Berkeley, California 94720, USA*
[2] *Dipartimento di Matematica e Fisica, Ennio de Giorgi, Universit del Salento, Lecce, Italy*
[3] *CNR Nanotec, Institute of Nanotechnology, via Monteroni, 73100, Lecce*
[4] *Dipartimento di Fisica, Università di Pavia, via Bassi 6, Pavia (IT)*
[5] *PRISM, Princeton Institute for the Science and Technology of Materials, Princeton University, Princeton, New Jersey 08540, USA*

Exciton-polaritons are hybrid light-matter states that arise from strong coupling between an exciton resonance and a photonic cavity mode. As bosonic excitations, they can undergo a phase transition to a condensed state that can emit coherent light without a population inversion. This aspect makes them good candidates for thresholdless lasers, yet short exciton-polariton lifetime has made it difficult to achieve condensation at very low power densities. In this sense, long-lived symmetry-protected states are excellent candidates to overcome the limitations that arise from the finite mirror reflectivity of monolithic microcavities. In this work we use a photonic symmetry protected bound state in the continuum coupled to an excitonic resonance to achieve state-of-the-art polariton condensation threshold in GaAs/AlGaAs waveguide. Most important, we show the influence of fabrication control and how surface passivation via atomic layer deposition provides a way to reduce exciton quenching at the grating sidewalls.

INTRODUCTION

Efficient low-threshold lasing is a long-sought goal for various applications spanning from integrated circuits to biological sensing [1, 2]. However, as of today the emission of coherent and monochromatic light has relied on population inversion, which requires to overcome a threshold excitation power to achieve lasing. A different approach exploits hybrid light-matter particles, known as exciton-polaritons[3, 4], which arise in a semiconductor when the energy exchange rate between a photon and an exciton is higher than their losses. These particles possess properties inherited from their photonic component, such as a small effective mass, and from their excitonic component such as high nonlinearities[5, 6] that can be further enhanced via dipolar interactions[7, 8]. All these properties make them interesting candidates for devices[9] such as optical transistors[10, 11], fast optical switches[12, 13], and electrically-injected light sources [14].

Because of their bosonic nature, they can undergo a phase transition to a coherent state, known as Bose-Einstein condensate[15, 16] (BEC), without the need for population inversion, making thresholdless lasing theoretically possible[17]. A necessary condition for this phase transition to happen is that the rate of scattering processes[18] that populate the BEC state must exceed the loss rates[9]. This has been one of the main limitations in the historical achievement of exciton-polariton condensates, as polaritons tend to accumulate in the so-called "bottleneck"[19, 20]. Such limitation was overcome by growing highly reflective mirrors with layers exceeding 40 pairs in both sides of a microcavity as well as using many stacks of QWs. In the last few years a different approach has enabled the achievement of polariton states in horizontal platforms[5, 21–25], making the fabrication easier and less time consuming. A similar waveguide configuration with multiple QWs was used to investigate the enhancement of dipolar polariton interactions[8, 26–28]. More recently, the same heterostructure led to the achievement of a Bose-Einstein condensate from a bound state in the continuum (BIC)[29] while also proving the topological charge possessed by the condensate. In this work we show the achievement of a low-density condensate in a GaAs/AlGaAs waveguide by tuning the parameters of a low-loss shallow grating and then we consider the effect of the reduction of excitonic losses on the threshold. In order to reduce the radiative losses we make use of a topologically protected bound state in the continuum [30–32] which is introduced in the polariton dispersion through the realization of a 1D etched grating[33]. Since the BIC has an antisymmetric profile, it cannot couple to outgoing plane waves, resulting in a perfectly dark state with zero radiative linewidth [34]. The exciton-polariton dispersion can be modified by changing the grating periodicity, which defines the energy at which the photonic modes cross. Such crossing can then be adjusted to bring the BIC closer to or further from the exciton, changing its excitonic fraction. This will ultimately change the threshold as the excitonic fraction has also an effect on the polariton thermalization towards the BIC. This control is something that has no

counterparts in classical vertical microcavities and can be tuned with extreme precision on several different gratings on the same chip. The excitonic fractions were estimated throughout this work by using the coupled oscillators model described in the supplementary materials.
A horizontal configuration and such long-lived state can drastically ease the fabrication with respect to vertical microcavities in order to achieve thermalization of polaritons into a single quantum state. Here we demonstrate the achievement of low-threshold condensate thanks to simple, yet extremely effective sample processing. We will consider three different shallow etched 1D gratings: 40nm, 90nm, and 130nm deep grooves. Finally, we show the reduction of the exciton-polariton linewidth and condensate threshold by passivating the trap states that form on the groove sidewalls during the etching process.

RESULTS

The sample is composed of a GaAs substrate on which a waveguide slab is grown via molecular beam epitaxy. 500nm of $Al_{0.8}Ga_{0.2}As$ are firstly grown onto the substrate, forming the waveguide cladding. A set of 12 GaAs quantum wells (QWs) and 13 $Al_{0.4}Ga_{0.6}As$ barriers 20nm thick were grown on top of the cladding, forming the waveguide core. Lastly, 10nm of GaAs were grown on top of the last barrier to act as a cap layer. The optical mode is confined in the waveguide core through total internal reflection, and here it exchanges energy with the QW excitons leading to propagating polaritons. A shallow etched 1D grating (Fig.1a) can be used to couple propagating and counterpropagating photonic modes via the slab refractive index modulation, hence we can easily introduce new properties by engineering the photonic dispersion. In our system we can exploit such coupling between photonic modes to introduce a symmetry protected bound state in the continuum which appears in the so-called dark state. If we consider E_{Bright} and E_{Dark} as the photonic modes originated from the grating coupling and separated by an energy gap, the energy exchange with the QWs exciton can lead to the following system Hamiltonian

$$H = \begin{pmatrix} E_{Bright} & \frac{\Omega}{2} & 0 & 0 \\ \frac{\Omega}{2} & X & 0 & 0 \\ 0 & 0 & E_{Dark} & \frac{\Omega}{2} \\ 0 & 0 & \frac{\Omega}{2} & X \end{pmatrix} \tag{1}$$

The photonic bright and dark states are then hybridized with the exciton, hence the diagonalization leads to exciton-polariton eigenstates with a BIC in the dark lower state (Fig.1b)[35]. Since the gap depends on the coupling strength between the photonic modes, it also depends on the grating's fabrication parameters, such as the etching depth and the filling factor, defined as $FF = 1 - \frac{\text{width}}{\text{pitch}}$ (Fig.1a). We used Stanford Stratified Structure Solver (S4) [36] to simulate the structure in Fig.1a, from which we obtained the energy dispersion shown in Fig.1b. The exciton was introduced in the simulations with a Lorentzian resonance in the GaAs dielectric constant, with a Rabi splitting $\Omega = 13.9$meV [8]. The bound state in the continuum appears as a saddle point of the dark state as shown in [29], which creates a direct path for polaritons to thermalize from the exciton reservoir.
The fabricated gratings are 50μm wide, 300μm long with a filling factor 70% - 75%. The periodicity was set around 240nm to have the photonic mode coupling close to the exciton resonance. We realized the grooves by writing an electron beam sensitive resist, and subsequent pattern transfer into the heterostructure via ICP-Chlorine etching[37–40]. The etched grating penetrated into the waveguide core, and three different depths were chosen, resulting in different degrees of photonic coupling.

The sample was cooled down to 4K in a cryostat and polaritons were created by nonresonantly pumping with a laser onto the grating (See Methods). Light was outcoupled by the grating itself and the energy dispersion imaged on a CCD camera. Accumulation of polaritons in the long-lived state triggers the onset of a coherent emission by bosonic stimulation. The polariton energy dispersion at and above threshold for a grating with filling factor FF = 75% is shown in Fig.2a and Fig.2b.

The power at which the condensation occurs was found to be strongly dependent on the grating parameters. Fig.3 shows the threshold intensity in a 90nm deep grating as a function of the periodicity. We chose gratings with periodicities equal to 240nm, 242nm, and 244nm which correspond to excitonic fractions 51.2%, 22.6%, and 12.1%, respectively. We observed a lower threshold for the 240nm pitch with respect to the 242nm and 244nm cases, ascribable to the higher exciton fraction. In our system, the grating periodicity moves the BIC closer to or further from the exciton, making the polariton thermalization process more or less efficient for the two cases.
In order to reduce the threshold, different etching depths d were studied with filling factors close to 70%: 40nm, 90nm, 130nm and the measured dispersions are reported in Fig.S6d-f. The etching is performed in the waveguide core, which has consequences on the polariton modes quality. The trap states in the electronic band gap created during the

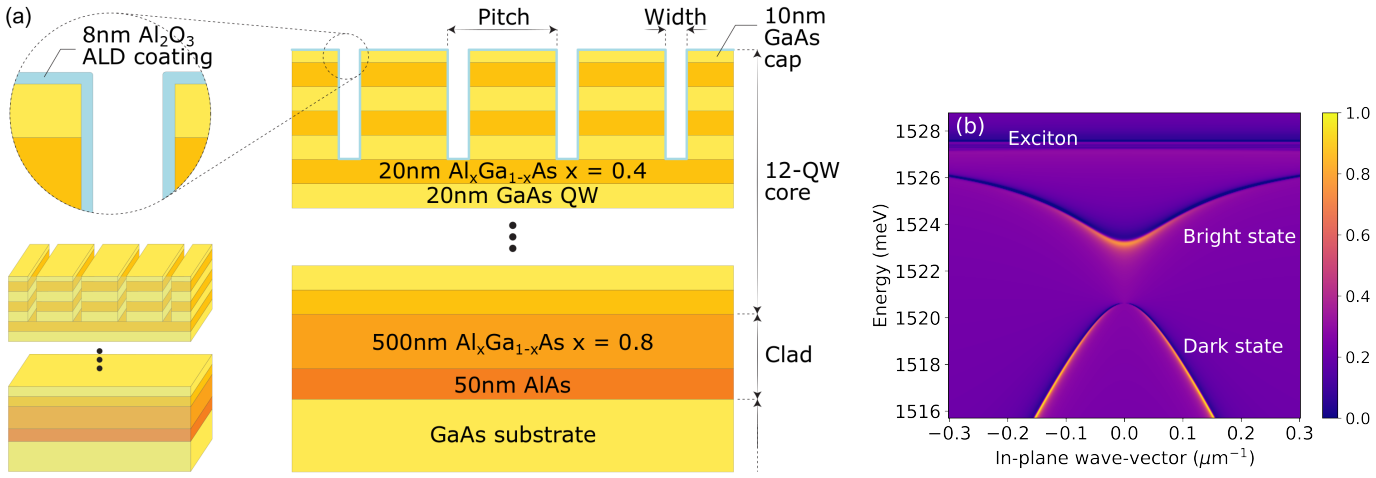

FIG. 1: (a) Sketch of the final processed waveguide sample with a 90nm deep grating, along with a conformal passivating layer of Al_2O_3. (b) Simulations of the exciton-polariton dispersion with bright and dark states coupled to the exciton. The BIC appears here as a dark state at the maximum energy point of the dispersion, corresponding to vertical emission ($k_{||} = 0$) in the far field.

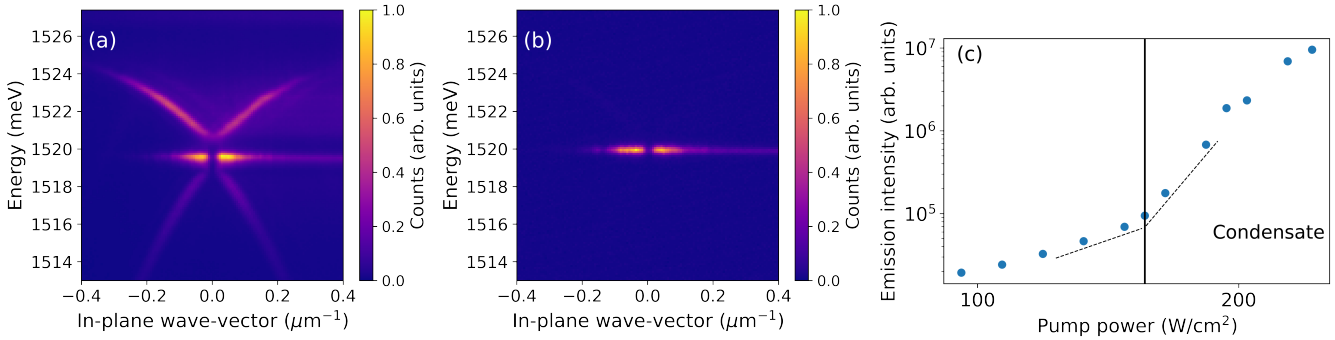

FIG. 2: (a,b) Exciton-polariton energy dispersion and coherent light emission at (a) and above (b) the excitation threshold. The condensate in (b) is blueshifted as a result of polariton-polariton interactions. (c) Emission intensity from the condensate as a function of the pumping power.

fabrication lead to nonradiative exciton surface recombination at the QWs sidewalls. Surface recombination can be minimized through oxide removal and surface passivation, achievable through etching at sufficiently low ion energy to remain in the ion-assisted chemical etching regime[41–43]. For this reason, the sample was immersed in a hydrochloric acid bath to remove the surface oxide, and then 8nm of Al_2O_3 were deposited via atomic layer deposition[44–47] (ALD) at 300C [48]. The observed intensity emission in the three cases along with the gap size and excitonic fraction are shown in Fig.4a,b. The lower threshold observed in deeper gratings is caused by a larger gap. In fact, the BIC state is more protected from the lossy bright state when the gap is larger. In other words, the smaller the gap, the closer the BIC is to the bright state, the higher the losses induced by leakage of the polariton population into the lossy state. Concurrently with the etching depth, the surface damage increases as demonstrated by the 130nm deep grating in which the condensate was achieved only from one structure with a high filling factor, and only after post-processing, as a consequence of a more pronounced damage (see Fig.S11). The damage induced by the etching was found to act mainly on the excitonic component, as shown in Fig.5 and it is discussed in the supplementary material where cathodoluminescence hyperspectral maps elucidate the effect of surface damage on the emission[49–51].

Lastly we observed the effect of post-processing on gratings characterized by 240nm pitch and 90nm deep grooves before and after passivation. The polariton dispersion for this grating is shown in Fig.5a and Fig.5b, where the threshold reached an energy per pulse corresponding to a few $\frac{\mu J}{cm^2}$ after ALD as displayed in Fig.5c. This measurement was performed on several gratings, and all of them showed the same characteristic reduction (See Fig.S10). The longer polariton lifetime, which we associate to lower nonradiative exciton recombination at the groove sidewalls, can be

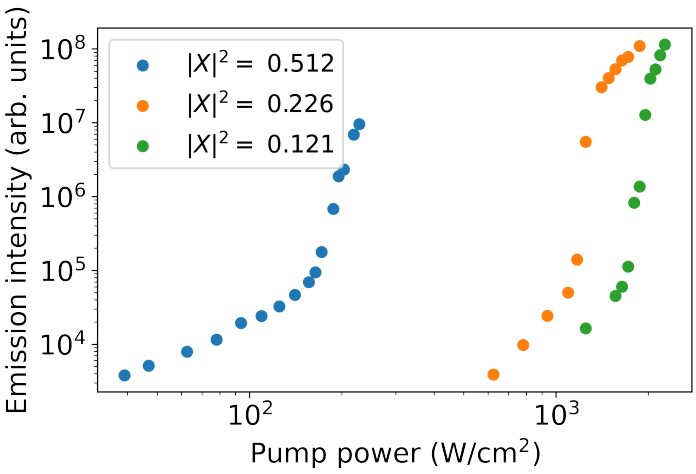

FIG. 3: Emission intensity from the condensate for periodicities 240nm (blue), 242nm (orange), and 244nm (green). The excitonic fraction $|X|^2$ is modified by the grating pitch, favoring a polariton thermalization towards the BIC and reducing the power threshold in the 240nm case.

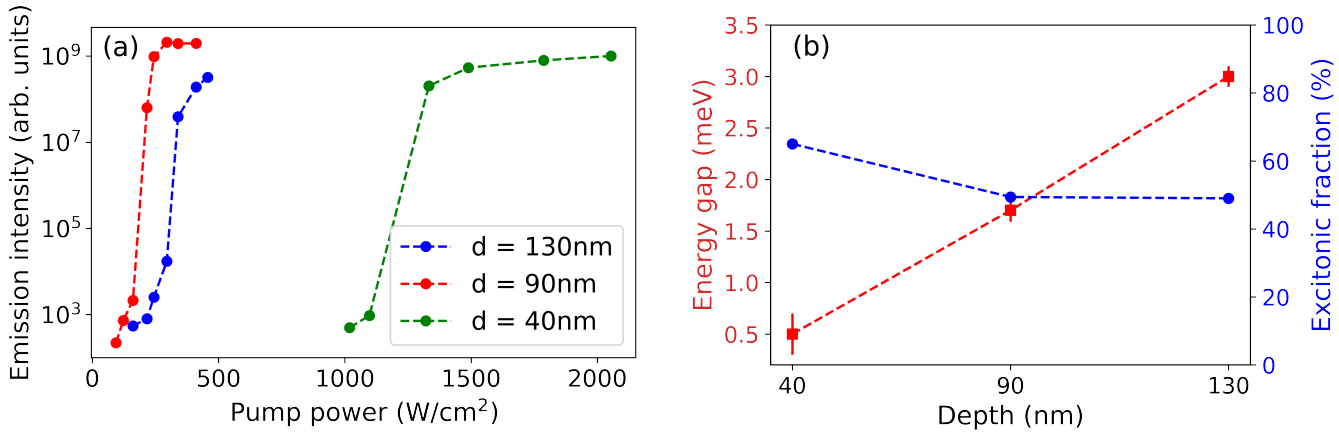

FIG. 4: (a) Emission intensity as a function of the pump power. The threshold is minimum for a grating 90nm deep, while it is higher for a 40nm deep grating due to smaller gap size, and for a 130nm deep grating due to surface damage. (b) Energy gap and excitonic fraction as a function of the etching depth. The filling factor is approximately the same in all the three cases.

observed in terms of linewidth reduction after Al_2O_3 deposition (Fig.5e). This result, even though limited by the spectrometer resolution and inhomogeneous broadening, clearly highlights the reduction of exciton inhomogeneous broadening which ultimately corresponds to a longer exciton-polariton lifetime. A more detailed discussion about the BIC lifetime is presented in [29] where a lower limit is set by means of polariton propagation under the grating. While the effect on the excitonic component is clear, no significant shift in the polariton dispersion was observed after the aluminum oxide deposition, a sign that the lower Al_2O_3 refractive index (n = 1.6 for thin film) compared to the photonic mode effective refractive index (n = 3.359) does not alter the designed structure behaviour.

CONCLUSIONS

The main limitation in achieving thresholdless exciton-polariton lasing is hindered by non-radiative and radiative losses that are inevitably present in microcavities. In this work we have realized a low-density exciton-polariton condensate in a horizontal cavity that makes use of the long lifetime of a quasi-bound state in the continuum in which

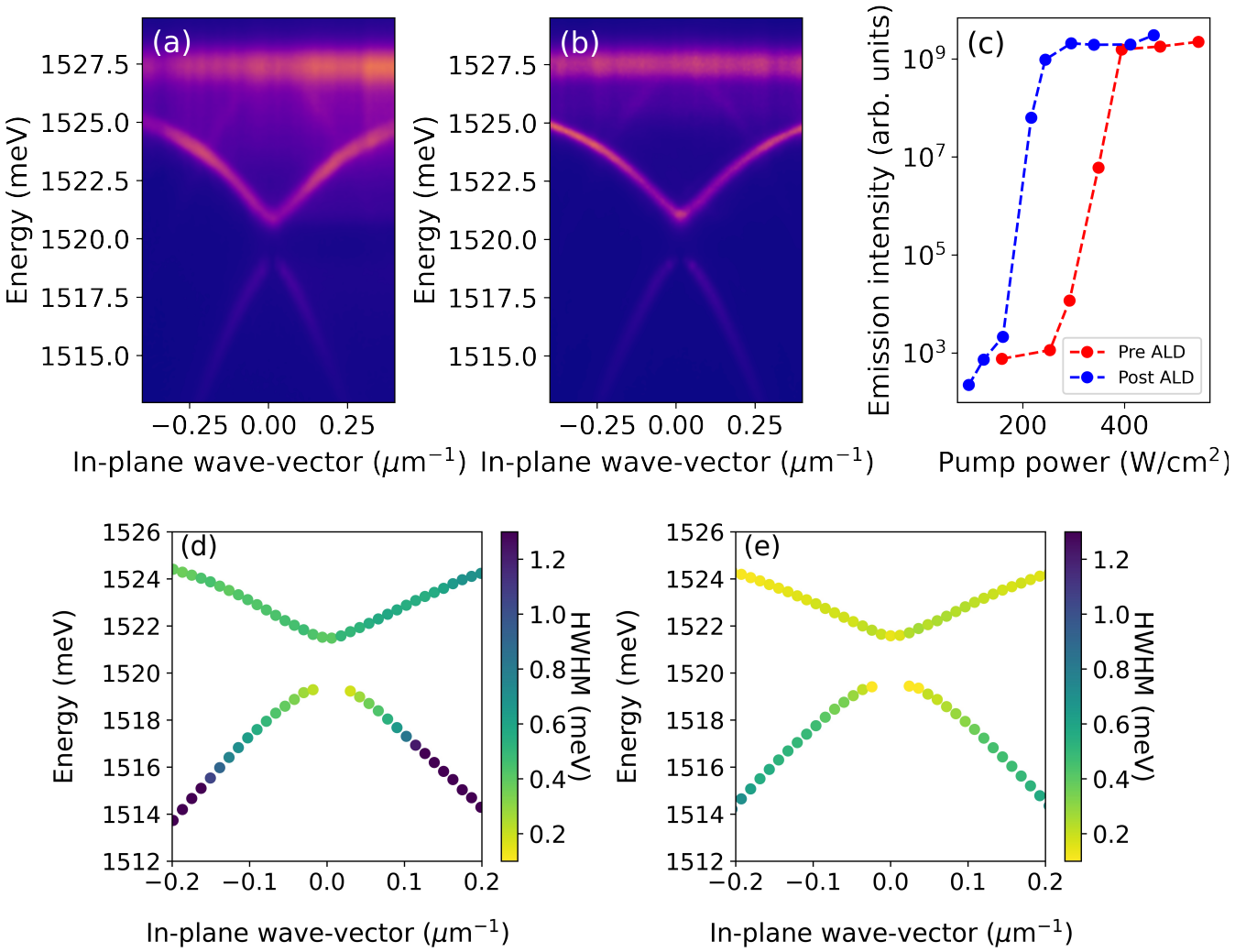

FIG. 5: (a,b) Exciton-polariton energy dispersion pre- and post-processing, respectively. (c) Lasing intensity measured at the threshold before and after aluminum oxide deposition for a 90nm deep grating, 240nm pitch. (d,e) Exciton-polariton dispersions corresponding to the case (a) and (b). Colors represent the HWHM fit of the linewidths.

lifetime is increased by several orders of magnitude due to the special nature of this dark state. However, surface damage during processing introduces nonradiative channels through which excitons can decay. By performing surface ALD post-processing we greatly reduce such an effect, increasing the polariton lifetime at the BIC. Our method substantially lowers the power needed to achieve a polariton condensate. This system is not only a good candidate for low threshold lasers, but also for those experiments that have been affected by the simultaneous presence of horizontal and vertical polariton lasing as recently reported in [22]. In conclusion we assessed the role of grating parameters and fabrication in the achievement of state-of-the-art polariton BEC arising from a bound state in the continuum coupled to an excitonic resonance. The extremely long lifetime of the polariton BIC facilitates the thermalization of the bosonic gas with the onset for condensation at a low polariton density despite the presence of lower energy states. Finally we also observed the reduction of the threshold and improvement in the polariton lifetime after hydrochloric acid and passivation of the sidewalls via atomic layer deposition, reducing the density of nonradiative recombination centers at the QW sidewalls. In the case of deep etching, the role of ALD was crucial, given it was able to restore the possibility to observe the condensate from one 130nm deep grating, while it reduced the threshold in all the 90nm deep gratings. The linewidth narrowing observed after post-processing is related to the reduction of non-radiative recombination, improving the overall quality factor of the sample leading to an estimated polariton lifetime of a few hundreds of picoseconds in the BIC[29]. Since BEC formation from a BIC has the great advantage of reaching the

phase transition at extremely low densities, it can be used to obtain ultra-low threshold lasers. The techniques and ideas investigated and developed here will not only boost the realization of polariton-based thresholdless lasers, but could also be a way to realize horizontal electrically pumped polariton light sources.

MATERIALS AND METHODS

Optical Measurements. The sample was kept at 4K for all the experiments. All measurements were performed using a 150fs, 80MHz pump laser with its central energy tuned at 1.588meV (780nm), and a spot size of 15μm FWHM. The emission from the sample was sent to a SpectraPro-300i spectrometer with a 1200lines/mm grating in order to reconstruct the reciprocal space. The optical setup allowed the simultaneous acquisition of Fourier space and real space images, which made it possible to keep the sample in focus at all times. To remove spurious effects, the laser tail was cut at around 800nm by a short pass filter, combined with a spatial filter which removes any emission outside the selected grating region.

Acknowledgments We are grateful to Ronen Rapaport for inspiring discussions and for sharing information about the sample design. The authors acknowledge the project PRIN Interacting Photons in Polariton Circuits INPhoPOL [Ministry of University and Scientific Research (MIUR), Grant No. 2017P9FJBS_001]. Work at the Molecular Foundry was supported by the Office of Science, Office of Basic Energy Sciences, of the U.S. Department of Energy under Contract No. DE-AC02-05CH11231. We acknowledge the project FISRC. N. R. Tecnopolo di nanotecnologia e fotonica per la medicina di precisioneCUP B83B17000010001 and Progetto Tecnopolo per la Medicina di precisione, Deliberazione della Giunta Regionale Grant No. 2117. This research is funded in part by the Gordon and Betty Moore Foundations EPiQS Initiative, Grant No. GBMF9615 to L. N. Pfeiffer, and by the National Science Foundation MRSEC Grant No. DMR 1420541. L. Francaviglia acknowledges funding from the Swiss National Science Foundation (SNSF) via Early PostDoc Mobility Grant No. P2ELP2_184398. Triennal Programm 2021 -2023. Italian Ministry of Research (MIUR) through the FISR 2020 COVID, project Sensore elettro-ottico a guida d'onda basato sull'interazione luce-materia (WaveSense), FISR2020IP_04324.

Disclosures The authors declare no conflicts of interest.

* daniele.sanvitto@nanotec.cnr.it

* daniele.sanvitto@nanotec.cnr.it

[1] R. M. Ma and R. F. Oulton, Applications of nanolasers, Nature Nanotechnology **14**, 12 (2019).
[2] M. T. Hill and M. C. Gather, Advances in small lasers, Nature Photonics **8**, 908 (2014).
[3] C. Weisbuch, M. Nishioka, A. Ishikawa, and Y. Arakawa, Observation of the coupled exciton-photon mode splitting in a semiconductor quantum microcavity, Physical Review Letters **69**, 3314 (1992).
[4] A. Kavokin, J. J. Baumberg, G. Malpuech, and F. P. Laussy, Microcavities (Oxford University Press, 2008) pp. 1–432.
[5] P. M. Walker, C. E. Whittaker, D. V. Skryabin, E. Cancellieri, B. Royall, M. Sich, I. Farrer, D. A. Ritchie, M. S. Skolnick, and D. N. Krizhanovskii, Spatiotemporal continuum generation in polariton waveguides, Light: Science & Applications **8**, 6 (2019).
[6] E. Estrecho, T. Gao, N. Bobrovska, D. Comber-Todd, M. D. Fraser, M. Steger, K. West, L. N. Pfeiffer, J. Levinsen, M. M. Parish, T. C. Liew, M. Matuszewski, D. W. Snoke, A. G. Truscott, and E. A. Ostrovskaya, Direct measurement of polariton-polariton interaction strength in the Thomas-Fermi regime of exciton-polariton condensation, Physical Review B **100**, 035306 (2019).
[7] E. Togan, H. T. Lim, S. Faelt, W. Wegscheider, and A. Imamoglu, Enhanced Interactions between Dipolar Polaritons, Physical Review Letters **121**, 227402 (2018).
[8] D. G. Suárez-Forero, F. Riminucci, V. Ardizzone, N. Karpowicz, E. Maggiolini, G. Macorini, G. Lerario, F. Todisco, M. D. Giorgi, L. Dominici, D. Ballarini, G. Gigli, A. S. Lanotte, K. West, K. Baldwin, L. Pfeiffer, and D. Sanvitto, Enhancement of Parametric Effects in Polariton Waveguides Induced by Dipolar Interactions, Physical Review Letters **126**, 137401 (2021).
[9] D. Sanvitto and S. Kéna-Cohen, The road towards polaritonic devices, Nature Materials **15**, 1061 (2016).
[10] D. Ballarini, M. De Giorgi, E. Cancellieri, R. Houdré, E. Giacobino, R. Cingolani, A. Bramati, G. Gigli, and D. Sanvitto, All-optical polariton transistor, Nature Communications **4**, 1778 (2013).

[11] C. Sturm, D. Tanese, H. Nguyen, H. Flayac, E. Galopin, A. Lemaître, I. Sagnes, D. Solnyshkov, A. Amo, G. Malpuech, and J. Bloch, All-optical phase modulation in a cavity-polariton MachZehnder interferometer, Nature Communications **5**, 3278 (2014).

[12] A. V. Zasedatelev, A. V. Baranikov, D. Sannikov, D. Urbonas, F. Scafirimuto, V. Y. Shishkov, E. S. Andrianov, Y. E. Lozovik, U. Scherf, T. Stöferle, R. F. Mahrt, and P. G. Lagoudakis, Single-photon nonlinearity at room temperature, Nature **597**, 493 (2021).

[13] D. G. Suárez-Forero, F. Riminucci, V. Ardizzone, A. Gianfrate, F. Todisco, M. De Giorgi, D. Ballarini, G. Gigli, K. Baldwin, L. Pfeiffer, and D. Sanvitto, Ultrafast, low-energy, all-optical switch in polariton waveguides, arXiv:2110.05704 (2021).

[14] C. Schneider, A. Rahimi-Iman, N. Y. Kim, J. Fischer, I. G. Savenko, M. Amthor, M. Lermer, A. Wolf, L. Worschech, V. D. Kulakovskii, I. A. Shelykh, M. Kamp, S. Reitzenstein, A. Forchel, Y. Yamamoto, and S. Höfling, An electrically pumped polariton laser, Nature **497**, 348 (2013).

[15] J. Kasprzak, M. Richard, S. Kundermann, A. Baas, P. Jeambrun, J. M. Keeling, F. M. Marchetti, M. H. Szymánska, R. André, J. L. Staehli, V. Savona, P. B. Littlewood, B. Deveaud, and L. S. Dang, Bose-Einstein condensation of exciton polaritons, Nature **443**, 409 (2006).

[16] T. Byrnes, N. Y. Kim, and Y. Yamamoto, Exciton-polariton condensates, Nature Physics **10**, 803 (2014).

[17] A. Imamoglu, R. J. Ram, S. Pau, and Y. Yamamoto, Nonequilibrium condensates and lasers without inversion: Exciton-polariton lasers, Physical Review A - Atomic, Molecular, and Optical Physics **53**, 4250 (1996).

[18] H. J. Miesner, D. M. Stamper-Kurn, M. R. Andrews, D. S. Durfee, S. Inouye, and W. Ketterle, Bosonic stimulation in the formation of a Bose-Einstein condensate, Science **279**, 1005 (1998).

[19] F. Tassone, C. Piermarocchi, V. Savona, and A. Quattropani, Bottleneck effects in the relaxation and photoluminescence of microcavity polaritons, Physical Review B - Condensed Matter and Materials Physics **56**, 7554 (1997).

[20] M. Richard, J. Kasprzak, R. André, R. Romestain, L. S. Dang, G. Malpuech, and A. Kavokin, Experimental evidence for nonequilibrium Bose condensation of exciton polaritons, Physical Review B **72**, 201301 (2005).

[21] O. Jamadi, F. Reveret, P. Disseix, F. Medard, J. Leymarie, A. Moreau, D. Solnyshkov, C. Deparis, M. Leroux, E. Cambril, S. Bouchoule, J. Zuniga-Perez, and G. Malpuech, Edge-emitting polariton laser and amplifier based on a ZnO waveguide, Light: Science & Applications **7**, 82 (2018).

[22] O. Jamadi, F. Réveret, D. Solnyshkov, P. Disseix, J. Leymarie, L. Mallet-Dida, C. Brimont, T. Guillet, X. Lafosse, S. Bouchoule, F. Semond, M. Leroux, J. Zuniga-Perez, and G. Malpuech, Competition between horizontal and vertical polariton lasing in planar microcavities, Physical Review B **99**, 085304 (2019).

[23] P. M. Walker, L. Tinkler, M. Durska, D. M. Whittaker, I. J. Luxmoore, B. Royall, D. N. Krizhanovskii, M. S. Skolnick, I. Farrer, and D. A. Ritchie, Exciton polaritons in semiconductor waveguides, Applied Physics Letters **102**, 012109 (2013).

[24] D. M. Di Paola, P. M. Walker, R. P. Emmanuele, A. V. Yulin, J. Ciers, Z. Zaidi, J. F. Carlin, N. Grandjean, I. Shelykh, M. S. Skolnick, R. Butté, and D. N. Krizhanovskii, Ultrafast-nonlinear ultraviolet pulse modulation in an AlInGaN polariton waveguide operating up to room temperature, Nature Communications **12**, 1 (2021).

[25] D. G. Suárez-Forero, F. Riminucci, V. Ardizzone, M. De Giorgi, L. Dominici, F. Todisco, G. Lerario, L. N. Pfeiffer, G. Gigli, D. Ballarini, and D. Sanvitto, Electrically controlled waveguide polariton laser, Optica **7**, 1579 (2020).

[26] I. Rosenberg, Y. Mazuz-Harpaz, R. Rapaport, K. West, and L. Pfeiffer, Electrically controlled mutual interactions of flying waveguide dipolaritons, Physical Review B **93**, 195151 (2016).

[27] I. Rosenberg, D. Liran, Y. Mazuz-Harpaz, K. West, L. Pfeiffer, and R. Rapaport, Strongly interacting dipolar-polaritons, Science Advances **4**, eaat8880 (2018).

[28] D. Liran, I. Rosenberg, K. West, L. Pfeiffer, and R. Rapaport, Fully Guided Electrically Controlled Exciton Polaritons, ACS Photonics **5**, 4249 (2018).

[29] V. Ardizzone, F. Riminucci, S. Zanotti, A. Gianfrate, M. Efthymiou-Tsironi, D. G. Suàrez-Forero, F. Todisco, M. De Giorgi, D. Trypogeorgos, G. Gigli, K. Baldwin, L. Pfeiffer, D. Ballarini, H. S. Nguyen, D. Gerace, and D. Sanvitto, Polariton BoseEinstein condensate from a bound state in the continuum, Nature **605**, 447 (2022).

[30] A. Kodigala, T. Lepetit, Q. Gu, B. Bahari, Y. Fainman, and B. Kanté, Lasing action from photonic bound states in continuum, Nature **541**, 196 (2017).

[31] C. W. Hsu, B. Zhen, A. D. Stone, J. D. Joannopoulos, and M. Soljačić, Bound states in the continuum, Nature Reviews Materials **1**, 16048 (2016).

[32] H. M. Doeleman, F. Monticone, W. Den Hollander, A. Alù, and A. F. Koenderink, Experimental observation of a polarization vortex at an optical bound state in the continuum, Nature Photonics **12**, 397 (2018).

[33] V. Kravtsov, E. Khestanova, F. A. Benimetskiy, T. Ivanova, A. K. Samusev, I. S. Sinev, D. Pidgayko, A. M. Mozharov, I. S. Mukhin, M. S. Lozhkin, Y. V. Kapitonov, A. S. Brichkin, V. D. Kulakovskii, I. A. Shelykh, A. I. Tartakovskii, P. M. Walker, M. S. Skolnick, D. N. Krizhanovskii, and I. V. Iorsh, Nonlinear polaritons in a monolayer semiconductor coupled to optical bound states in the continuum, Light: Science & Applications **9**, 56 (2020).

[34] B. Zhen, C. W. Hsu, L. Lu, A. D. Stone, and M. Soljačić, Topological Nature of Optical Bound States in the Continuum, Physical Review Letters **113**, 257401 (2014).

[35] L. Lu, Q. Le-Van, L. Ferrier, E. Drouard, C. Seassal, and H. S. Nguyen, Engineering a lightmatter strong coupling regime in perovskite-based plasmonic metasurface: quasi-bound state in the continuum and exceptional points, Photonics Research **8**, A91 (2020).

[36] V. Liu and S. Fan, S 4: A free electromagnetic solver for layered periodic structures, Computer Physics Communications **183**, 2233 (2012).

[37] Z. Liao and J. S. Aitchison, Precision etching for multi-level AlGaAs waveguides, Optical Materials Express **7**, 895 (2017).
[38] T. Maeda, J. W. Lee, R. J. Shul, J. Han, J. Hong, E. S. Lambers, S. J. Pearton, C. R. Abernathy, and W. S. Hobson, Inductively coupled plasma etching of III-V semiconductors in BCl3-based chemistries. I. GaAs, GaN, GaP, GaSb and AlGaAs, Applied Surface Science **143**, 174 (1999).
[39] X. Zhou, I. Kulkova, T. Lund-Hansen, S. L. Hansen, P. Lodahl, and L. Midolo, High-efficiency shallow-etched grating on GaAs membranes for quantum photonic applications, Applied Physics Letters **113**, 1 (2018).
[40] K. A. Atlasov, P. Gallo, A. Rudra, B. Dwir, and E. Kapon, Effect of sidewall passivation in BCl3/N2 inductively coupled plasma etching of two-dimensional GaAs photonic crystals, Journal of Vacuum Science & Technology B: Microelectronics and Nanometer Structures **27**, L21 (2009).
[41] O. J. Glembocki, J. A. Tuchman, K. K. Ko, S. W. Pang, A. Giordana, R. Kaplan, and C. E. Stutz, Effects of electron cyclotron resonance etching on the ambient (100) GaAs surface, Applied Physics Letters **66**, 3054 (1995).
[42] D. Leonhardt, C. R. Eddy, V. A. Shamamian, R. T. Holm, O. J. Glembocki, and J. E. Butler, Surface chemistry and damage in the high density plasma etching of gallium arsenide, Journal of Vacuum Science & Technology A: Vacuum, Surfaces, and Films **16**, 1547 (1998).
[43] C. R. Eddy, O. J. Glembocki, D. Leonhardt, V. A. Shamamian, R. T. Holm, B. D. Thoms, J. E. Butler, and S. W. Pang, Gallium arsenide surface chemistry and surface damage in a chlorine high density plasma etch process, Journal of Electronic Materials **26**, 1320 (1997).
[44] B. Guha, F. Marsault, F. Cadiz, L. Morgenroth, V. Ulin, V. Berkovitz, A. Lemaître, C. Gomez, A. Amo, S. Combrié, B. Gérard, G. Leo, and I. Favero, Surface-enhanced gallium arsenide photonic resonator with quality factor of 6 10ˆ6, Optica **4**, 218 (2017).
[45] C. L. Hinkle, A. M. Sonnet, E. M. Vogel, S. McDonnell, G. J. Hughes, M. Milojevic, B. Lee, F. S. Aguirre-Tostado, K. J. Choi, H. C. Kim, J. Kim, and R. M. Wallace, GaAs interfacial self-cleaning by atomic layer deposition, Applied Physics Letters **92**, 071901 (2008).
[46] D. Mikulik, A. C. Meng, R. Berrazouane, J. Stückelberger, P. RomeroGomez, K. Tang, F. Haug, A. Fontcuberta i Morral, and P. C. McIntyre, Surface Defect Passivation of Silicon Micropillars, Advanced Materials Interfaces **5**, 1800865 (2018).
[47] V. Dhaka, A. Perros, S. Naureen, N. Shahid, H. Jiang, J.-P. Kakko, T. Haggren, E. Kauppinen, A. Srinivasan, and H. Lipsanen, Protective capping and surface passivation of III-V nanowires by atomic layer deposition, AIP Advances **6**, 015016 (2016).
[48] I. V. Levitskii, M. I. Mitrofanov, G. V. Voznyuk, D. N. Nikolaev, M. N. Mizerov, and V. P. Evtikhiev, Annealing of FIB-Induced Defects in GaAs/AlGaAs Heterostructure, Semiconductors **52**, 1898 (2018).
[49] M. Negri, L. Francaviglia, D. Dumcenco, M. Bosi, D. Kaplan, V. Swaminathan, G. Salviati, A. Kis, F. Fabbri, and A. Fontcuberta I Morral, Quantitative Nanoscale Absorption Mapping: A Novel Technique to Probe Optical Absorption of Two-Dimensional Materials, Nano Letters **20**, 567 (2020).
[50] P. Hovington, D. Drouin, and R. Gauvin, CASINO: A new Monte Carlo code in C language for electron beam interaction - Part I: Description of the program, Scanning **19**, 1 (1997).
[51] D. Drouin, A. R. Couture, D. Joly, X. Tastet, V. Aimez, and R. Gauvin, CASINO V2.42 - A fast and easy-to-use modeling tool for scanning electron microscopy and microanalysis users, Scanning **29**, 92 (2007).